*High Power Laser Science and Engineering*, (2024), Vol. 12, e72, 9 pages.
doi:10.1017/hpl.2024.72

HIGH POWER LASER SCIENCE AND ENGINEERING

RESEARCH ARTICLE

# 10 GeV proton generation driven by 5 PW light spring pulses

Yi Guo[1], Xiaomei Zhang[1], Baifei Shen[1], and Toshiki Tajima[2]

[1] *Department of Physics, Shanghai Normal University, Shanghai, China*

[2] *Department of Physics and Astronomy, University of California, Irvine, California, USA*

*(Received 8 October 2024; accepted 11 October 2024)*

**Abstract**

Proton acceleration in a near-critical-density gas driven by a light spring (LS) pulse with a helical structure in its intensity profile is investigated using three-dimensional particle-in-cell simulations. Compared with other pulse modes with the same laser power, such as the Gaussian pulse or the donut Laguerre–Gaussian (LG) pulse, the LS structure significantly enhances the peak intensity and drives a stronger longitudinal acceleration field and transverse focusing field. Both the high intensity and helical structure of the LS pulse contribute to the formation of a bubble-like structure with a fine electron column on the axis, which is critical for stable proton acceleration. Therefore, it is very promising to obtain ultra-high-energy protons using LS pulses with a relatively lower power. For example, by using LS pulses with the same power of 4.81 PW, the proton in the gas can be accelerated up to 8.7 GeV, and the witness proton can be accelerated to 10.6 GeV from 0.11 GeV, which shows the overwhelming advantage over the Gaussian and LG pulse cases.

**Keywords:** 10 GeV; light spring; proton acceleration; wakefield

## 1. Introduction

High-energy ion beams can be used in a wide range of fields[1–3]. Laser-driven acceleration is an attractive approach to obtain high-energy protons. Along with the completion of 10 PW laser constructions, such as the ELI-NP and SULF facilities, the record of proton energy has broken through 100 MeV based on the target normal sheath acceleration (TNSA) scheme or a hybrid mechanism in several laboratories[4]. However, it is still very challenging to further increase the proton energy because of the rigorous requirement for the experimental conditions. Nevertheless, a higher proton energy, such as a few GeV or tens of GeV, is a long-term goal for the attractive prospects.

In recent years, the radiation pressure acceleration (RPA) scheme has become an efficient way to acquire high-energy protons[5–9]. Theoretically, this method can produce protons with energy in the GeV range. However, it remains difficult to further increase the proton energy to several GeV through RPA because of the decreasing acceleration gradient when the accelerated proton velocity is approaching the speed of light[10]. Moreover, a large focus spot is necessary for long-term acceleration of the RPA, which implies that a high laser power is required. To obtain a higher-energy (above 10 GeV) proton beam, the acceleration field should move at near-light speed along with the proton beam[11–14]. This implies that the wakefield or bubble structure is a good option for producing ultra-high-energy proton beams, which has been confirmed by numerous theoretical studies[13,15–18]. However, there are two necessary conditions for proton wakefield acceleration. One is the ultra-high intensity/power of the driving laser pulse. Current research results show that protons can be self-injected in the wakefield driven by a Gaussian (GS) laser only when the laser intensity is about $10^{23}$ W/cm$^2$, corresponding to a laser power of 100 PW[15], because a large focus size is required. Although for the external injection of protons, the laser intensity should still be of the order of $10^{22}$ W/cm$^2$, corresponding to a laser power in the range of tens of petawatts[12], such high power is still difficult to achieve and is unavailable in real experiments for current laser facilities. Furthermore, in a regular bubble driven by a GS laser pulse, the transverse field has a defocusing effect

Correspondence to: X. Zhang and B. Shen, Department of Physics, Shanghai Normal University, Shanghai 200234, China. Emails: zhxm@shnu.edu.cn (X. Zhang); bfshen@shnu.edu.cn (B. Shen)

on the positively charged particles and scatters them to the bubble sheath. Therefore, the protons cannot be well-confined in the acceleration field. It has been found that, when a vortex laser with a donut structure in the intensity distribution, such as the Laguerre–Gaussian (LG) laser, propagates in undersense plasma, a bubble structure with an electron pillar on the axis can be formed[16,19–21]. This special structure can confine protons in the plasma near the bubble axis, resulting in continuous and stable proton acceleration.

The light spring (LS) laser is a new type of space–time coupled laser that can be composed of several LG laser pulses with different frequencies and topological charges[22]. The most prominent features of such a laser are the spiral structure of the phase and intensity contours. Unlike the LG pulse with a donut intensity distribution, the high-intensity bright spot of the LS pulse is concentrated within a small arc of the ring, and the intensity at other positions on the ring is extremely low (almost zero). That is, as the LS pulse propagates forward, the position of the high-intensity bright spot rotates around the optical axis[22,23]. In recent experiments, an LS with arbitrary topological-spectral correlations has been realized by employing a diffractive axicon with a circular geometry that imparts azimuthal phase modulations to the beams[24]. This LS pulse with a highly focused intensity at a specific local position has a significantly increased peak intensity when compared to GS or LG pulses with the same power. Considering the current difficulty in constructing high-power petawatt lasers, this provides a feasible prospect for ultra-high-energy proton acceleration with moderate power lasers.

In this study, this special vortex pulse propagating in a near-critical-density plasma is investigated using three-dimensional particle-in-cell (3D PIC) simulations. It is found that, when the LS pulse, even at a relatively low power, interacts with the under-dense plasma, a bubble-like structure with an electron pillar on the optical axis forms spontaneously. Protons in the background plasma can be trapped and stably accelerated for a long time. Simulation results show that a proton beam can be accelerated to 8.7 GeV by 4.81 PW LS laser pulses. The proton energy is increased by about 10 times when compared to the acceleration effect of the LG and GS pulses at the same power, in which cases there are no self-injected protons. Considering the cascade acceleration of protons, the witness proton can be accelerated to 10.6 GeV from 0.11 GeV, which significantly eases the trapping condition.

## 2. Theoretical analysis

Physically, LS pulses can be created by combining multiple LG pulses. Actually, coherent beam combining is widely used to produce high-intensity laser beams[25,26]. An LG beam with the number of radial nodes $p = 0$ can be expressed as $a_{\mathrm{LG}}(r,\theta,t) = a_{\mathrm{r}}(r)\ \exp\ (i(l\theta - \omega t)) = a_0\left(\sqrt{2}/w_z\right)^{|l|}\exp\left(-r^2/w_z^2\right)\exp(i(l\theta - \omega t))$, where $a_{\mathrm{r}}(r)$ denotes the transverse laser profile, $l$ denotes the topological charge, $z_{\mathrm{R}}$ denotes the Rayleigh distance and $w_z = w_0\sqrt{\left(z^2+z_{\mathrm{R}}^2\right)/\left(z_{\mathrm{R}}^2\right)}$, where $w_0$ denotes the beam-waist radius. The position of the maximum radial intensity of the LG beam is at $r = \sqrt{w_0^2 l/2}$, which is related to the topological charge. In this study, to increase the coherence of the superposition beams and make the bright spot more concentrated, the waist radius of each LG beam $w_{01}\sqrt{l_1} = w_{0n}\sqrt{l_n}$, where $w_{0n}$ denotes the beam-waist radius of the $n$th beamlet with a topological charge $l_n$. Each LG mode with a different topological charge is associated with a specific frequency[22,27]. The LS pulse synthesized by $N$ beams of the LG pulse with intensity $a_0$ is described as follows:

$$\begin{aligned} a_{\mathrm{LS}}(r,\theta,t) &= \sum_{n=1}^{N} a_{\mathrm{LG}}(r,\theta,t) \\ &= \sum_{n=1}^{N} a_0\left(\frac{\sqrt{2}}{w_{zn}}\right)^{|l_1|}\exp\left(-\frac{r^2}{w_{zn}^2}\right)\exp(i(l_n\theta - \omega_n t)), \end{aligned} \tag{1}$$

where $l_n = l_1 + \Delta l(n-1)$, $\omega_n = \omega_1 + \Delta\omega(n-1)$, $w_{zn} = w_{0n}\sqrt{\left(z^2+z_{\mathrm{R}}^2\right)/\left(z_{\mathrm{R}}^2\right)}$, $\Delta\omega$ denotes the bandwidth gap and $\Delta l$ denotes the topological charge gap.

The intensity of such beam is as follows:

$$I_{\mathrm{LS}} = a_{\mathrm{LS}}(r,\theta,t)\cdot a_{\mathrm{LS}}(r,\theta,t)^* = a_{\mathrm{r}}^2(r)\frac{\sin^2\left(\frac{N\Delta l(\theta-\alpha\omega_0 t)}{2}\right)}{\sin^2\left(\frac{\Delta l(\theta-\alpha\omega_0 t)}{2}\right)}, \tag{2}$$

where $\alpha\omega_0 = \Delta\omega/\Delta l$ and $\omega_0$ denotes the central frequency. Equation (2) indicates that the intensity profile of the LS pulse is helical. The interference effect causes the light intensity to concentrate around a specific angle $\theta_0$. The high-intensity bright spot rotates around the laser axis, forming a spring-like intensity contour in space and time. When $\Delta l = 1$, the angular position of the peak intensity is $\theta_0(t,z) = \alpha\omega_0(t - z/c)$ and pitch $p = \lambda/\alpha$, where $\lambda$ is the central wavelength.

It is well known that for a laser pulse, intensity $I_0$ is proportional to amplitude $a_0{}^2$, with $I_0 = Ca_0^2$, where $C = 1.37 \times 10^{18}\ (\mathrm{W/cm^2})/\lambda^2$. According to Equation (2), the intensity of the LS pulse synthesized by $N$ LG beams with $a_0$ can be expressed as $I_{\mathrm{LS}} = CN^2a_0^2$ and power $P_{\mathrm{LS}} = N\int Ca_0^2\mathrm{d}s$, resulting from the power sum of $N$ beams. However, when an LG pulse has the same power as an LS pulse, its peak intensity can be expressed as $I_{\mathrm{LG}} = CNa_0^2$. Therefore, at the same power, the LS pulse achieves a peak

https://doi.org/10.1017/hpl.2024.72 Published online by Cambridge University Press

laser intensity $N$ times higher than that of the LG pulse (i.e., the amplitude is $N^{1/2}$ times higher), which implies significant advantages in terms of particle acceleration.

## 3. Three-dimensional particle-in-cell simulation results

Proton acceleration driven by the LS pulse was demonstrated using 3D PIC simulations based on EPOCH code[28]. The simulation box has dimensions 80 μm ($x$) × 60 μm ($y$) × 60 μm ($z$), corresponding to a moving window with 1000 × 800 × 800 cells and one particle per cell. The tritium low-density plasma, doped with a small amount of hydrogen, occupies the 10 μm < $x$ < 800 μm region in the propagation direction of the laser pulse, and –27 μm < $y$ ($z$) <27 μm. The density of electron $n_e = 1.23 \times 10^{27}$ m$^{-3}$ and the density ratio of tritium to hydrogen particles is 70:1. The slow-moving massive background tritium ions enable the formation of a stable electron bubble with a large space-charge field[15], which facilitates the stable generation of accelerating bubbles in the plasma and benefits the acceleration of protons. The LS pulse is composed of seven LG pulses with different topological charges, ranging from $l_1 = 1$ to $l_7 = 7$, and a frequency spacing of $\alpha\omega_0 = 0.05\omega_0$. The central wavelength $\lambda = 0.8$ μm. The detailed numerical values of the seven pulses are listed in Table 1, where the waist radius of each LG beam $w_{01}\sqrt{l_1} = w_{0n}\sqrt{l_n}$ is satisfied to increase the coherence of the superposition beams and make the bright spot more concentrated, where $w_{0n}$ denotes the beam-waist radius of the $n$th beamlet with a topological charge $l_n$. The normalized peak amplitude of the sub-LG beam $a_{LG} = 15$; thus, the normalized peak amplitude of the synthesized LS pulse is expected to be $a_{LS} = 105$. The pulse duration of the sub-beams $T = 16$ μm, equal to the pitch of the LS pulse.

It should be noted that the transverse intensity distribution of the LG pulse has a donut-like structure, so that an electron column which is critical for the transverse confinement of protons can be generated when it propagates in the gaseous plasma. For an LS pulse with helical structure intensity, it also has a singular point at the center of the pulse, similar to the LG pulse. However, the symmetry of its transverse distribution is weakened; it is difficult to form a straight electron column because of the asymmetric ponderomotive force on the background electrons. To increase the symmetry of the induced bubble-like structure and obtain a stable electron column, two LS pulses with high-intensity bright spots symmetrically positioned relative to the central axis were used. In fact, this structure is the same as that of an LS pulse with $\Delta l = 2$.

The 3D PIC simulation results are shown in Figure 1. As shown in Figures 1(a) and 1(b), when two LS pulses propagate in low-density plasma, the ponderomotive force of the spring-like electric field expels and spirals electrons outward, forming a bubble-like structure with an electron column on the central axis, which results in a focusing effect for the positively charged particles[19,20]. It is well known that when the laser intensity is sufficiently high, protons in the background plasma can be trapped by the intense longitudinal acceleration field and move with the bubble structure for further acceleration. The maximum strength of the normalized electric field is $a_{LS} \simeq 100$, as shown in Figure 1(c), for the reason of the good energy concentration of the high-intensity bright spot. However, the power is only 4.81 PW, which is one to two orders of magnitude lower than the previously reported value (it should be noted that for the same laser strength and focus spot, protons cannot be well-accelerated by RPA for a general GS pulse). The high intensity of the LS pulse contributes to the generation of the intense acceleration field, as shown in Figure 1(d), which is critical for proton injection and acceleration. With the

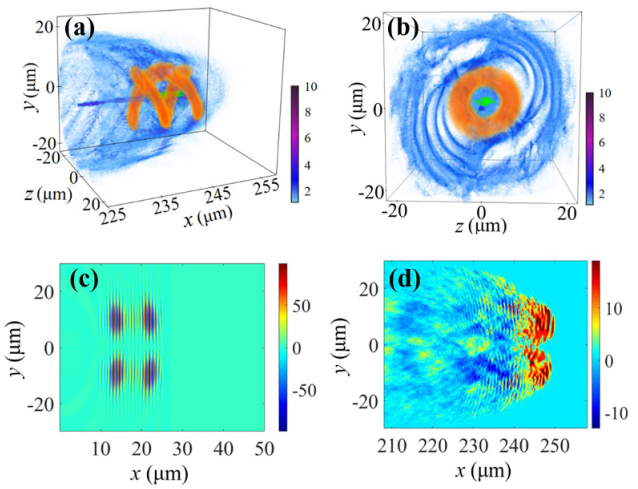


**Figure 1.** At $t = 862$ fs, (a) side view and (b) frontal view of the LS pulse (orange), high-density protons (green) and electrons (blue/purple) from different views. At this time, the field of the LS pulse is considerably weakened. The color bar represents electron density, which is normalized to $n_c$. (c) At $t = 92$ fs, the electric field distribution of the LS pulse $E_y$ in the $x$–$y$ plane at $z = 0$. (d) Acceleration field $E_x$ in the $x$–$y$ plane at $z = 0$ and $t = 862$ fs. The electric field is normalized to $m_e\omega_0 c/e$.

**Table 1.** Topological charge $l_n$ of the $n$th LG sub-beam constituting the synthesized LS pulse, and the corresponding beam-waist radius $w_{0n}$ and angular frequency $\omega_n$.

| Sub-beam number $n$ | 1 | 2 | 3 | 4 | 5 | 6 | 7 |
|---|---|---|---|---|---|---|---|
| Topological charge $l_n$ | 1 | 2 | 3 | 4 | 5 | 6 | 7 |
| Angular frequency $\omega_n$ | $0.85\omega_0$ | $0.9\omega_0$ | $0.95\omega_0$ | $\omega_0$ | $1.05\omega_0$ | $1.1\omega_0$ | $1.15\omega_0$ |
| Waist radius $w_{0n}$ (μm) | 16 | 11.314 | 9.238 | 8 | 7.155 | 6.532 | 6.047 |

https://doi.org/10.1017/hpl.2024.72 Published online by Cambridge University Press

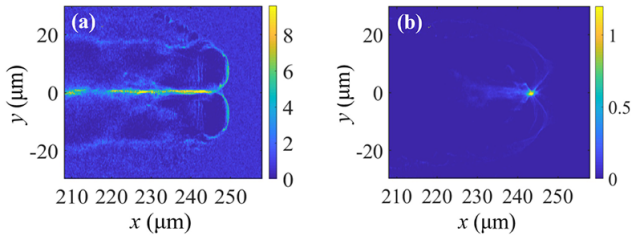


**Figure 2.** (a) Electron density and (b) proton density in the $x$–$y$ plane at $z = 0$ and $t = 862$ fs.

present parameters, the protons were trapped in the bubble-like structure and well-confined by the electron column.

Figure 2 shows the electron and proton densities of the bubble-like structure in the $x$–$y$ plane at $z = 0$. It can be clearly observed that there is a thin electron column with a high density in the center of the structure. The protons are focused toward the electron column and accumulate at the head of the bubble-like structure, where the acceleration field is much stronger.

The trapped protons are confined to the axis and obtain high energy from the acceleration field. As shown in Figure 3(a), protons with higher momentum are located near the central axis, corresponding to protons with high density as shown in Figure 2(b). Based on the energy spectral distribution of the protons, as shown in Figure 3(b), the cutoff energy reaches 8.7 GeV after about 1 ps acceleration with the energy conversion efficiency of 11% for protons exceeding 0.5 GeV. The proton energy spectrum is broad for the self-injection case because protons are trapped continuously from the background plasma, whereas protons with higher energy have smaller divergence angles, and the mean divergence angle is small (1.853°), as shown in Figure 3(c), which is important for applications. Here we should note that protons no more than 1 GeV have been obtained for GS pulses even though the same effective spot size of 4 μm at the same power has been used, and no better acceleration results can be obtained for the pure RPA by the GS pulse with such a small focal spot.

## 4. Discussion

### *4.1. Detailed comparison of simulation results and the trapping condition*

The initial energy of the trapped protons depends on the potential of the bubble structure. The Hamiltonian of a proton in the wakefield and electromagnetic field is $h_0 = \sqrt{1 + p_x^2 + \rho_p^2 a^2} - \rho_p \phi(\xi) - v_p P_x$, where $\xi = x - ct$, and $h_0$ is an integration constant corresponding to the initial proton condition in front of the bubble. For a proton initially at rest, $h_0 = 1$. Here, $v_p$ is the bubble velocity, $P_x = \gamma v_x$ is the proton longitudinal momentum, $v_x$ is the proton velocity, $\rho_p = -1/1836$, $\phi(\xi) = \int E_x d\xi$ is the scalar potential and $E_x$ is the acceleration field, which is positively correlated with $\sqrt{a_0}$. According to the simulation results of the acceleration field for the LS pulse case, the maximum potential $\phi_{max} \simeq 1305$. It is well known that, if the scalar potential is sufficiently high, then the protons can be accelerated to a speed equal to the bubble velocity, resulting in proton trapping. The trapping conditions are expressed as follows:

$$h_0 + \rho_p \phi_{trap} = 1/\gamma_p.$$

The potential required for trapping $\phi_{trap} = 1260$, which is smaller than the maximum potential for the LS pulse case and, thereby, protons can be trapped in the bubble-like structure. The motion of the protons can be expressed as follows:

$$P_x = \frac{v_p(\rho_p\phi(\xi) + h_0) + \sqrt{(\rho_p\phi(\xi) + h_0)^2 - (1 - v_p^2)(1 - (\rho_p\phi(\xi) + h_0)^2)}}{1 - v_p^2}. \quad (3)$$

From Equation (3), the proton momentum that can be achieved after acceleration at different wakefield velocities is as shown in Figure 4. According to the simulation results, the average velocity of the bubble-like structure is $v_p = 0.971c$,

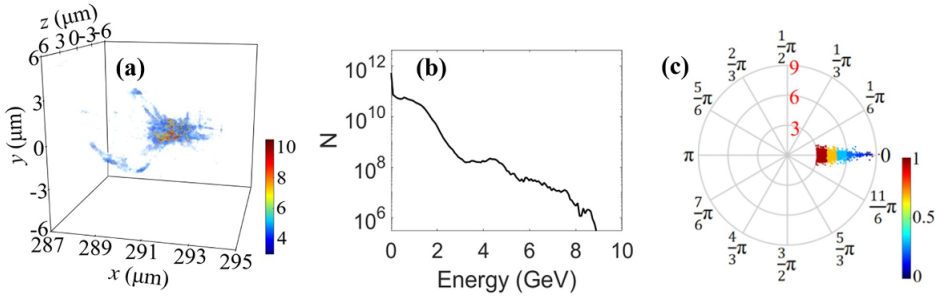


**Figure 3.** (a) At $t = 1.02$ ps, longitudinal momentum distributions of protons, with the momentum normalized to $m_p c$ and $m_p$ denoting the proton mass. (b) Energy spectra of protons and (c) angular distribution of proton energy, where the color bar represents the number of protons normalized to the maximum number of protons.

https://doi.org/10.1017/hpl.2024.72 Published online by Cambridge University Press

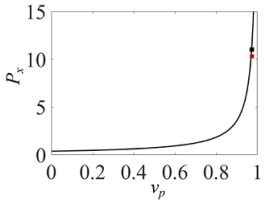


**Figure 4.** Dependence of proton momentum on the bubble velocity, where $v_p$ is normalized to $c$, and $P_x$ is normalized to $m_p c$. The black square indicates the theoretical result, and the red square indicates the simulation result.

corresponding to a Lorentz factor of $\gamma_p = 4.18$. The expected momentum is $10.96 m_p c$, which is in good agreement with the simulation result of $P_x = 10.31 m_p c$.

The spiral structure of the LS pulse results in a concentration of the laser intensity in the angular direction. That is, for the LS pulse, the high-intensity bright spot rotates around the laser axis, forming a spring-like intensity contour in space and time. When it propagates in the under-dense plasma, the bright spot pushes the dense electrons forward at a certain location in the cross-section, and at the next moment, the following bright spot pushes the fresh dense electrons at the other corresponding location. Therefore, the electron bubble-like structure in the LS pulse case is driven by the whole pulse instead of the pulse front as in the GS or LG cases. Meanwhile, both the high intensity and the helical structure of the LS pulse contribute to the formation of a bubble-like structure with a fine electron column on the axis, which is critical for stable proton acceleration. The electron column along the propagation axis results from the special ponderomotive force on the background electrons because the ponderomotive force has a corresponding structure with the helical intensity.

As mentioned above, there are two key stages for obtaining high-energy protons: the injection stage and the continuous acceleration stage. The LS pulse exhibits a spring-like intensity distribution. This structure significantly enhances the peak intensity by $N$ times and benefits both stages when compared with other modes, such as GS and LG pulses with the same power. The higher laser intensity $I$ implies a stronger ponderomotive force and drives a stronger longitudinal acceleration field $E_x$. To confirm this, the LG pulse and GS pulse with the same power of 4.81 PW as the driving pulse are used to compare the proton acceleration effect. The comparison of the driving field and acceleration field of the three cases is shown in Figure 5. In the LG case, the normalized amplitude is approximately 43, which is slightly

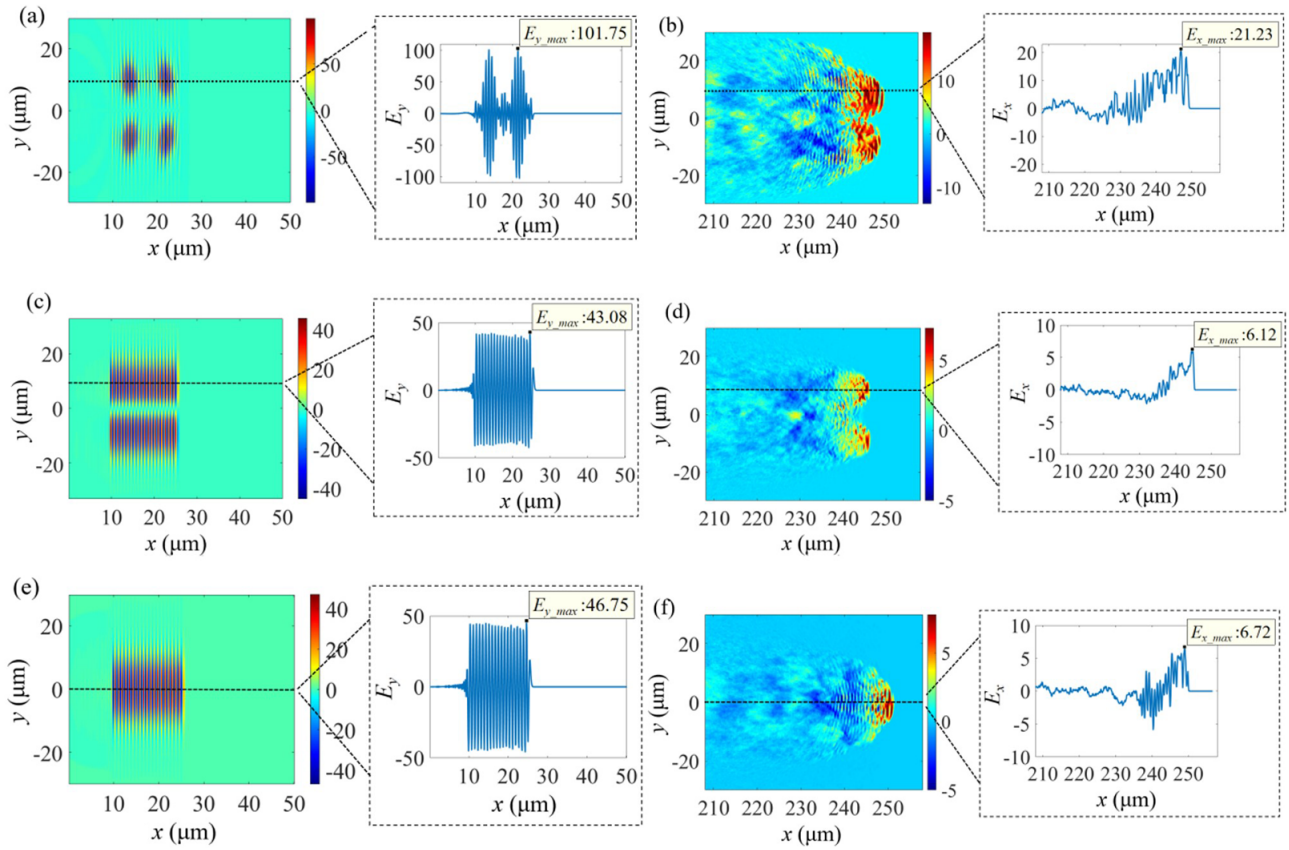


**Figure 5.** At $t = 92$ fs, electric field distribution of (a) the LS pulse, (c) the LG pulse and (e) the GS pulse in the $x$–$y$ plane at $z = 0$. The black line represents the selection of the line for the one-dimensional plot of the electric field. At $t = 862$ fs, acceleration field of (b) the LS pulse, (d) the LG pulse and (f) the GS pulse in the $x$–$y$ plane at $z = 0$. The black line represents the selection of the line for the one-dimensional plot of the acceleration field.

https://doi.org/10.1017/hpl.2024.72 Published online by Cambridge University Press

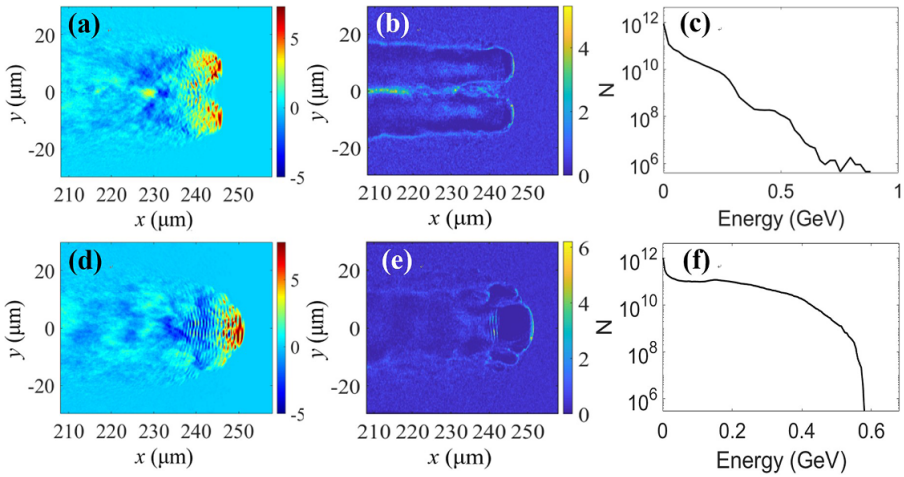


**Figure 6.** At $t = 862$ fs, the acceleration field of (a) the LG pulse and (d) the GS pulse. Electron density in the cases of (b) the LG pulse and (e) the GS pulse in the $x$–$y$ plane at $z = 0$. At $t = 1.02$ ps, the energy spectra of protons driven by (c) the LG pulse and (f) the GS pulse.

lower than the expected value according to $I_{LG} = 2I_{LS}/N$ (here, the coefficients of two results from two LS pulses are used in the PIC simulations). In the case of the GS pulse, the normalized amplitude is approximately 47. Apart from the driving pulse, the other parameters are the same as those in the case of the LS. As shown in Figures 6(a) and 6(b), the electron column is loose and insufficiently dense to confine protons. The peak intensity of the acceleration field for the LG pulse is $E_{xLG} = 6.1$, corresponding to the maximum potential $\phi_{max} = 335$, which is much lower than $\phi_{trap}$. The protons cannot be trapped and are continuously accelerated by the wakefield. As shown in Figures 6(d) and 6(e), the normalized peak intensity of the acceleration field for the GS pulse is $E_{xGS} = 6.7$. Due to the absence of a hollow ring structure in the vortex pulse, it fails to form a bubble structure with a central electron column near the axis. The protons diffuse gradually and do not accelerate well. As shown in Figures 6(c) and 6(f), the cutoff energy of the protons is much lower than 1 GeV for both the LG and GS pulse cases. In other words, LS pulses are overwhelmingly superior in proton acceleration.

### *4.2. Acceleration for the external injection*

Accelerating protons through self-injection is a simple and direct method that is relatively easy to implement in experiments. Here, a well-confined acceleration of the externally injected protons in the wakefield driven by the LS laser pulse is also considered. The same normalized amplitude $a_{LS} \simeq 100$ and power $P = 4.81$ PW were maintained consistent with the above self-trapped case. The tritium plasma with a density of $n_0 = 6.9 \times 10^{26}$ m$^{-3}$ occupies the same simulation box. The witness proton beam with a size of 4 μm × 2 μm × 2 μm is emitted from $x = 5$ μm and $y = z = 0$ μm. For comparison, a 4.81 PW LG pulse and a 4.81 PW GS pulse were used to accelerate the witness protons.

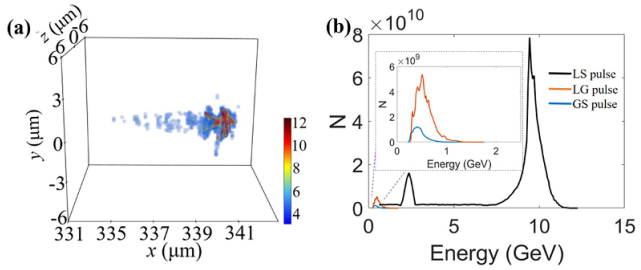


**Figure 7.** (a) At $t = 1.17$ ps, 3D longitudinal momentum distributions of witness protons for the LS pulse as the driving pulse. (b) Energy spectra of witness protons driven by LS, LG and GS pulses, respectively.

The other parameters were identical to those used in the LS acceleration case. As shown in Figure 7(a), the witness protons driven by the LS pulse are well-confined along the axis and effectively accelerated. The maximum momentum is $12.36 m_p c$ at $t = 1.17$ ps. Figure 7(b) shows the energy spectra of the witness protons driven by different laser pulses at $t = 1.17$ ps. For the LS pulse, the witness protons are accelerated to over 10 GeV from 0.11 GeV with an energy spread of 0.671°. In the cases of LG and GS pulses, most of the protons cannot be trapped and further accelerated by the wakefield. Hence, they significantly lag behind the moving bubble-like structures. Notably, cascaded proton acceleration has been reported for the well-known TNSA, collisionless electrostatic shock acceleration and RPA[29–31]. However, for the former two schemes, the energy gain within a few MeV to tens of MeV is limited because of the immovable or nonrelativistic acceleration field, whereas for the latter, the energy of the witness protons should be sufficiently high so that protons can follow the fast acceleration field.

### *4.3. Effective acceleration driven by the imperfect LS pulse*

We should note that, even though for the imperfect LS pulse, which is usually more possible to reach considering

https://doi.org/10.1017/hpl.2024.72 Published online by Cambridge University Press

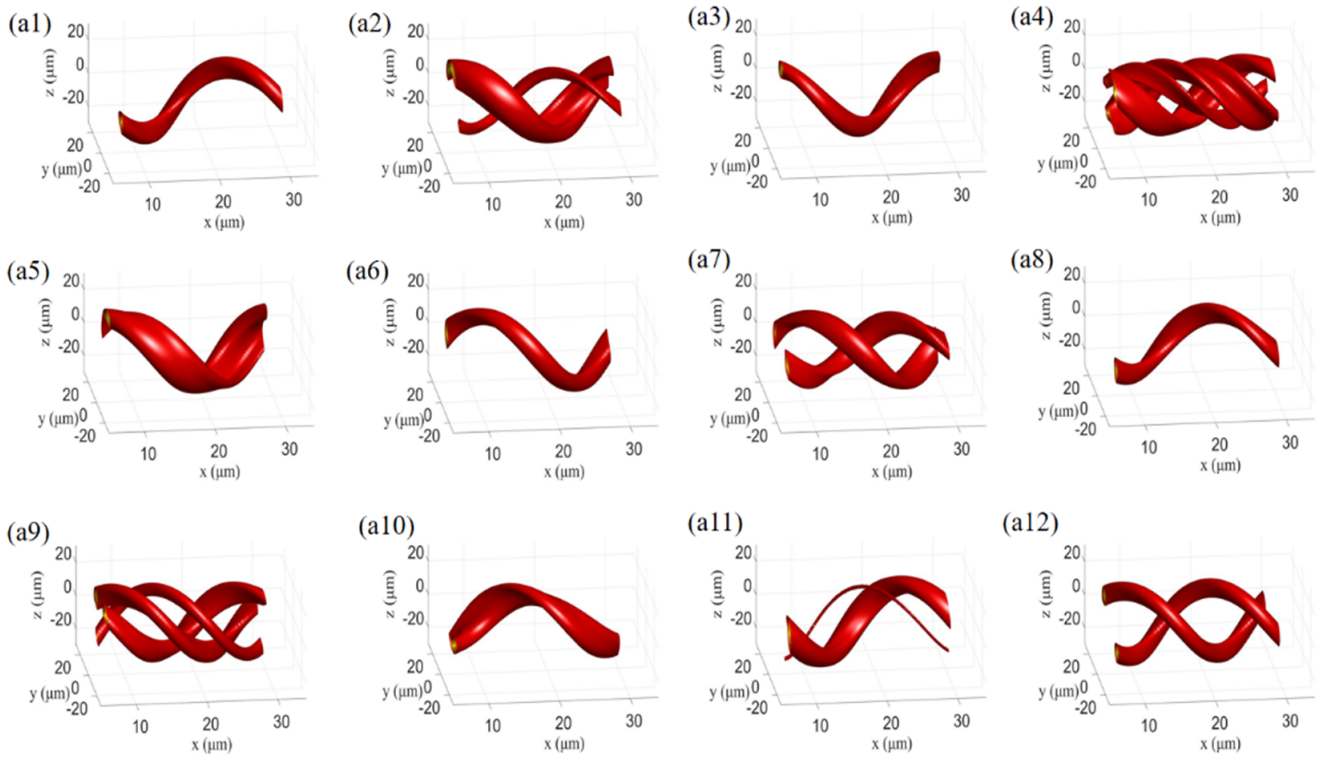


**Figure 8.** Intensity patterns for imperfect LS pulses combined by sub-LG beams with random initial phases in 12 simulation runs.

the current experimental technology, the results still show overwhelming advantages in proton acceleration compared with the LG pulse case.

Considering the feasible method of realization in the real experiments, the LS can be created by combining LG beamlets. If the phase and frequency of the LG beamlet are well controlled before combination, a perfect LS pulse with one strong point of time-dependent intensity can be obtained. Otherwise, an imperfect LS pulse with several strong points of time-dependent intensity owing to the random phase will be obtained. Considering the current experimental technology, the latter is usually more prone to be achieved. Therefore, besides the perfect LS case, we have performed the imperfect LS case by adding some random phases between the LG beamlets, and similar results are observed for the imperfect LS case. The probability of effective proton acceleration in the imperfect cases is 25% based on three cycles of effective acceleration in the 12 simulation runs with different random phases adding to the sub-LG beams in each run. The normalized peak amplitude of the sub-LG beam $a_{\mathrm{LG}} = 24$ and the total power is 12.3 PW (the peak intensity of the LS pulse after the incoherent superposition in the imperfect LS case is lower than that in the perfect LS case, so here higher total power is required to accelerate protons effectively). The other parameters of the driving laser and plasma are the same as that in the perfect LS case. As shown in Figures 8–10, protons can still be trapped by the wakefield and continuously accelerated for a long time, and eventually gain a cutoff energy up to 8.73 GeV, as shown in Figure 10(a). The acceleration process is similar to that in the perfect LS case, as shown in Figure 9.

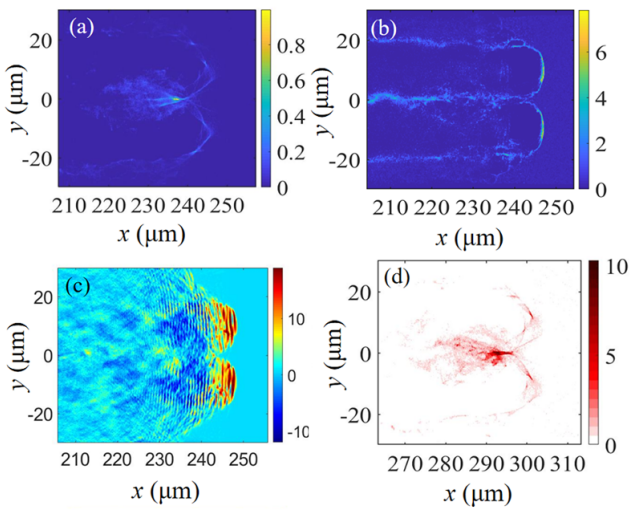


**Figure 9.** (a) Proton density, (b) electron density and (c) acceleration field $E_x$ in the $x$–$y$ plane at $z = 0$ and $t = 862$ fs when the imperfect LS pulse in Figure 8(a12) (combined by sub-LG beams with random initial phases) is used. The proton and electron density has been normalized to $n_{\mathrm{c}}$. The electric field is normalized to $m_{\mathrm{e}}\omega_0 c/e$. (d) At $t = 1.05$ ps, longitudinal momentum distributions of protons in the $x$–$y$ plane at $z = 0$, with the momentum normalized to $m_{\mathrm{p}}c$ and $m_{\mathrm{p}}$ denoting the proton mass.

https://doi.org/10.1017/hpl.2024.72 Published online by Cambridge University Press

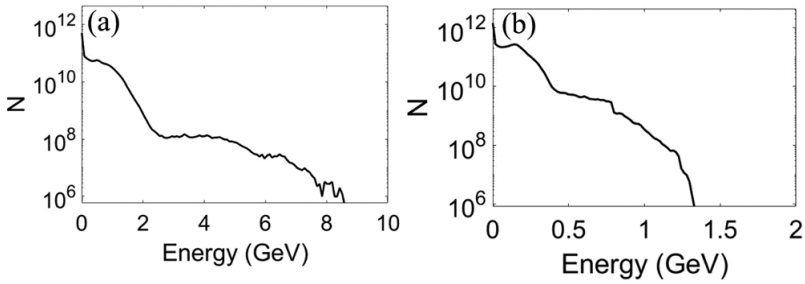


**Figure 10.** At $t = 862$ fs, the energy spectra of protons accelerated by (a) the imperfect LS laser pulse in Figure 8(a12) and (b) the LG laser pulse at the same power.

As comparison, in the case of the LG pulse at the same power of 12.3 PW, protons cannot be efficiently trapped due to the insufficient intensity, and the proton cutoff energy reaches 1.32 GeV, as shown in Figure 10(b), which is similar to the acceleration case in Figure 8(a4). Therefore, although a higher laser power such as 12.3 PW is required, the results still show overwhelming advantages in proton acceleration compared with the LG pulse case.

## 5. Conclusion

In summary, the proton acceleration in a bubble structure driven by an ultra-intense LS pulse was examined. Unlike the traditional hollow vortex beam, the LS pulse displays a spiral intensity profile, resulting in a higher peak intensity at a lower driving power, thus forming a bubble-like structure with an electron pillar on the $x$-axis. Owing to the sufficiently intense acceleration field in the longitudinal direction and focusing field in the transverse direction, protons can be effectively injected and accelerated. The 3D PIC simulation results show that, when two LS light pulses are symmetrical with respect to the central axis and have a total power of 4.81 PW, the peak intensity reaches $2.15 \times 10^{22}$ W/cm$^2$. When they interact with near-critical-density plasma, the protons in the background are well-trapped and confined near the axis of the acceleration bubble. After long-distance acceleration, the trapped protons obtain the energy of 8.7 GeV, showing an overwhelming advantage over the GS and LS pulses. It should be noted that the intensity can be enhanced $N$ times for the LS pulse when compared with that for the general GS or LG pulse at the same power. Therefore, there is huge potential for particle acceleration with a high $N$, even though the total power is not too high.

## Acknowledgement

This work was supported by the National Natural Science Foundation of China (Nos. 12475247, 11935008 and 12305274).

## References

1. M. Roth, T. E. Cowan, M. H. Key, S. P. Hatchett, and H. Powell, Phys. Rev. Lett. **86**, 436 (2001).
2. V. D. Shiltsev, Phys.-Usp. **55**, 965 (2012).
3. T. Esirkepov, S. V. Bulanov, K. Nishihara, and T. Tajima, Phys. Rev. Lett. **92**, 255001 (2004).
4. T. Ziegler, I. Göthel, S. Assenbaum, C. Bernert, F.-E. Brack, T. E. Cowan, N. P. Dover, L. Gaus, T. Kluge, S. Kraft, F. Kroll, J. Metzkes-Ng, M. Nishiuchi, I. Prencipe, T. Püschel, M. Rehwald, M. Reimold, H.-P. Schlenvoigt, M. E. P. Umlandt, M. Vescovi, U. Schramm, and K. Zeil, Nat. Phys. **20**, 1211 (2024).
5. B. Shen and Z. Xu, Phys. Rev. E **64**, 056406 (2001).
6. T. Esirkepov, M. Borghesi, S. V. Bulanov, G. Mourou, and T. Tajima, Phys. Rev. Lett. **92**, 175003 (2004).
7. B. Qiao, M. Zepf, M. Borghesi, and M. Geissler, Phys. Rev. Lett. **102**, 145002 (2009).
8. X. Q. Yan, H. C. Wu, Z. M. Sheng, J. E. Chen, and J. Meyer-Ter-Vehn, Phys. Rev. Lett. **103**, 135001 (2009).
9. A. Macchi, High Power Laser Sci. Eng. **2**, e10 (2014).
10. X. Zhang, B. Shen, L. Ji, W. Wang, J. Xu, Y. Yu, and X. Wang, Phys. Plasmas **18**, 073101 (2011).
11. B. Shen, X. Zhang, Z. Sheng, M. Y. Yu, and J. Cary, Phys. Rev. Spec. Top. Accel. Beams **12**, 121301 (2009).
12. L.-L. Yu, H. Xu, W.-M. Wang, Z.-M. Sheng, B.-F. Shen, W. Yu, and J. Zhang, New J. Phys. **12**, 045021 (2010).
13. X. Zhang, B. Shen, L. Ji, F. Wang, M. Wen, W. Wang, J. Xu, and Y. Yu, Phys. Plasmas **17**, 123102 (2010).
14. M. A. Bake, Z. Shan, B.-S. Xie, X.-R. Hong, and H.-Y. Wang, Phys. Plasmas **19**, 083103 (2012).
15. B. Shen, Y. Li, M. Y. Yu, and J. Cary, Phys. Rev. E **76**, 055402 (2007).
16. X. Zhang, B. Shen, L. Zhang, J. Xu, X. Wang, W. Wang, L. Yi, and Y. Shi, New J. Phys. **16**, 123051 (2014).
17. B. Rau, T. Tajima, and H. Hojo, Phys. Rev. Lett. **78**, 3310 (1997).
18. T. Tajima, X. Q. Yan, and T. Ebisuzaki, Rev. Mod. Plasma Phys. **4**, 7 (2020).
19. J. Vieira and J. T. Mendonça, Phys. Rev. Lett. **112**, 215001 (2014).
20. J. T. Mendonça and J. Vieira, Phys. Plasmas **21**, 033107 (2014).
21. X. Wang, B. Shen, X. Zhang, W. Wang, J. Xu, L. Yi, and Y. Shi, Phys. Plasmas **22**, 043106 (2015).
22. G. Pariente and F. Quere, Opt. Lett. **40**, 2037 (2015).
23. J. Vieira, J. T. Mendonca, and F. Quere, Phys. Rev. Lett. **121**, 054801 (2018).
24. M. Piccardo, M. de Oliveira, V. R. Policht, M. Russo, B. Ardini, M. Corti, G. Valentini, J. Vieira, C. Manzoni, G. Cerullo, and A. Ambrosio, Nat. Photonics **17**, 822 (2023).

https://doi.org/10.1017/hpl.2024.72 Published online by Cambridge University Press

25. G. Mourou, B. Brocklesby, T. Tajima, and J. Limpert, Nat. Photonics **7**, 258 (2013).
26. X. Guo, X. Zhang, D. Xu, W. Chen, Y. Guo, K. Lan, and B. Shen, Sci. Rep. **13**, 1104 (2023).
27. Y. Guo, X. Zhang, D. Xu, X. Guo, B. Shen, and K. Lan, Matter Radiat. Extrem. **8**, 035902 (2023).
28. C. Nieter and J. R. Cary, J. Comput. Phys. **196**, 448 (2004).
29. S. M. Pfotenhauer, O. Jäckel, J. Polz, S. Steinke, H. P. Schlenvoigt, J. Heymann, A. P. L. Robinson, and M. C. Kaluza, New J. Phys. **12**, 103009 (2010).
30. T. J. Xu, B. F. Shen, X. M. Zhang, L. Q. Yi, W. P. Wang, L. G. Zhang, J. C. Xu, X. Y. Zhao, Y. Shi, C. Liu, and Z. K. Pei, Phys. Plasmas **22**, 073101 (2015).
31. Z. Pei, B. Shen, X. Zhang, W. Wang, L. Zhang, L. Yi, Y. Shi, and Z. Xu, Phys. Plasmas **22**, 073113 (2015).

https://doi.org/10.1017/hpl.2024.72 Published online by Cambridge University Press